Journal of Sol-Gel Science and Technology (2022) 102:279–287
https://doi.org/10.1007/s10971-022-05744-w

ORIGINAL PAPER: SOL-GEL, HYBRIDS AND SOLUTION CHEMISTRIES

Room temperature synthesis of lanthanum phosphates with controlled nanotexture as host for Ln(III) through the *Epoxide Route*

Paula Borovik[1,2] · Víctor Oestreicher[1,2,3] · Paula C. Angelomé[2] · Beatriz C. Barja[1] · Matías Jobbágy[1]

Received: 23 August 2021 / Accepted: 15 February 2022 / Published online: 25 March 2022

Abstract

Herein, the *Epoxide Route*, a one-pot room temperature alkalinization method based on the reaction between a nucleophile and an epoxide, has been employed to synthesize $LaPO_4$ in the form of a *Rhabdophane* phase. The intrinsic features of this synthetic approach allow the reaction to be followed by pH monitoring, making possible the identification of the different precipitation steps involved in the formation of the solid. Once demonstrated the effectiveness of this chemical methodology, the size and shape of the $LaPO_4$ particles were controlled by varying the identity and proportion of the organic co-solvents employed to perform the reaction. By these means, crystalline particles with dumbbell, urchin and needle shapes were obtained, with sizes that ranged from less than 200 nm to more than 5 µm. Finally, luminescent materials in the form of a $LnPO_4$ *Rhabdophane* structure were easily obtained by the incorporation of Eu^{III} along the whole composition range. Additionally, photophysical characterization of selected samples was performed, with a promising outcome. The results presented in this work pave the way to obtaining a wide variety of luminescent materials with sizes and morphologies adjustable on demand, by using a simple and reliable synthetic approach.

Graphical abstract

The Epoxide Route has been adapted to drive the precipitation of lanthanum phosphates exhibiting high control on size and morphology through a solvent-controlled growth approach. Additionally, this synthetic scenario allows the obtaining of luminescent materials by simply incorporating Eu(III) in the whole composition range.

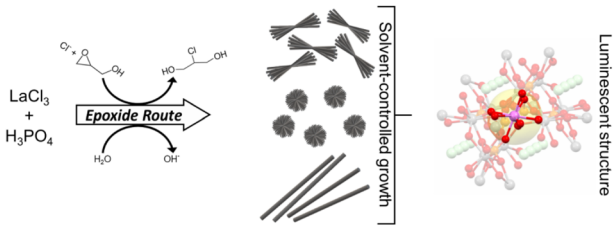

Keywords Lanthanide phosphates · Luminescent materials · Room temperature synthesis · Epoxide route

Supplementary information The online version contains supplementary material available at https://doi.org/10.1007/s10971-022-05744-w.

✉ Víctor Oestreicher
victor.oestreicher@uv.es

[1] INQUIMAE-DQIAQF, Facultad de Ciencias Exactas y Naturales, Universidad de Buenos Aires, Ciudad Universitaria, Pab. II (1428), Buenos Aires, Argentina

[2] Gerencia Química & Instituto de Nanociencia y Nanotecnología, Centro Atómico Constituyentes, Comisión Nacional de Energía Atómica, CONICET, Av. Gral. Paz 1499, San Martín (1650), Buenos Aires, Argentina

[3] Present address: Instituto de Ciencia Molecular (ICMol), Universidad de Valencia, Catedrático José Beltrán 2, Paterna (46980), Valencia, Spain

Highlights

- Room temperature synthesis of pure crystalline lanthanum phosphate is achieved.
- Particle size and shape can be easily controlled by using green organic co-solvents.
- $La_{1-x}Eu_xPO_4$ phases can be obtained in the whole composition range, yielding luminescent materials.

1 Introduction

Luminescent compounds based on rare-earth metals belong to a versatile group of functional materials. In particular, lanthanide-based compounds have application in a wide variety of fields, from drug-delivery and biosensing devices, to agriculture applications and laser industry uses [1–5]. In this sense, phosphate lattices and rare-earth ion's partnership has enabled the development of uncountable new research lines as diverse as the versatility these ions offer [6, 7]. In fact the diversity in the chemistry observed in the rare-earth phosphates has been exploited to such an extent that now these materials have found their niches of opportunity in many technologically relevant applications [8]. These include their use as insulating ceramics, ionic conductors, catalysts, dielectrics [9] and for nuclear waste treatment [10]. Given the unique luminescent properties of the rare-earth ions posses, perhaps the most exploited area is that related to their stable optical properties. As a consequence of their $4f^n$ configuration, each rare-earth ion displays a specific fingerprint of narrow intra $f-f$ emission bands, almost independent of the chemical environment. Luminescent rare-earth doped materials do not suffer from undesired photo-bleaching or photo-blinking which makes them suitable for use as lasers [11], scintillating or lighting materials, and even for applications that require upconversion processes [12]. In particular, the optical and luminescent properties of many rare-earth-doped phosphates have been extensively studied, for a wide range of structures and compositions both in bulk and in the nanoscale [13, 14]. Of these, Eu^{III} doped $LaPO_4$ compounds are amongst the most studied luminescent materials [15]. Firstly, $LaPO_4$ is chosen because of its low toxicity, good biocompatibility, high chemical, and thermal stability and its inherent capability to host other Ln^{III} ions [16]. Specifically, its f^0 configuration considerably diminishes the possibilities to cause deactivation due to crossed relaxation with the host Ln^{III}. In line manner, it is desirable that the matrix could act as an antenna to the phosphorus Ln^{III}, improving the material's luminescence. Furthermore, Eu^{III} is generally used as dopant because of its prominent emission when irradiated with UV light. Additionally, its emission spectrum is strongly influenced by the symmetry of the crystalline site the ion occupies, so it acts as probe of the nearest neighbourgs [17, 18].

Traditionally, synthetic methods used to obtain $LaPO_4$-based materials include hydrothermal recrystallization and/or thermal decomposition [19, 20]. These techniques ensure a high luminescence, chemical stability and enhanced crystallization, resulting, in most of the cases, in the isolation of the most thermodynamically stable phases. However, in some cases, soft crystallization methods are excellent complementary approaches, not only because they could favor the quantitative precipitation of pure metastable phases but also because they allow a fine tuning of morphology/shape and size. In this context, a distinct polarized emission taking place in $LaPO_4$ containing Eu^{III} nanorods has recently been reported. Thus, a straightforward synthetic method allowing control over the size and morphology of rare-earth-based phosphates would be very convenient [21].

For that reason, during the last few years, we have been intensely working on the development of the *Epoxide Route* [22], a one-pot homogeneous alkalinization method taking place at room temperature. Specifically, the main reaction involves the nucleophilic attack of an anion over an epoxide (chloride and glycidol, respectively), resulting in the net generation of hydroxyl moieties (Scheme 1). This approach has been successfully employed for the synthesis of several materials [23, 24] such as layered hydroxides [25], either in the form of purely inorganic [26] and hybrid phases [27, 28], a plethora of layered double hydroxides (LDHs) [29, 30], hydrogels [31], metal organic frameworks [32], gold nanoparticles [33], and more recently calcium phosphate phases [34]. However, beyond the possibility of synthesizing all of these materials, the most characteristic feature of the *Epoxide Route* is the possibility of performing in situ experiments thanks to the inherently mild conditions

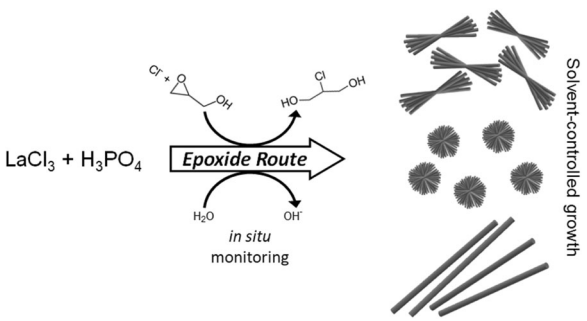

Scheme 1 Schematic representation of the strategy followed in this work. The *Epoxide Route* was optimized to study the precipitation of lanthanum phosphate phases, and additionally by employing our formerly solvent-controlled growth pathway, the size (from the nano to the micro scale) and morphology (from dumbbells- to urchin- and needle-like) can be easily tuned

at which the alkalinization and subsequent precipitation processes occur. By doing such studies, the understanding of precipitation mechanisms and phase stabilities, and even the role of different stabilizing agents over the materials formation, has been achieved.

Herein, we introduce the use of the *Epoxide Route* for the synthesis of a $LaPO_4$ *Rhabdophane* phase at room temperature, allowing us to assess the precipitation pathway for the first time. Additionally, by taking advantage of our solvent-controlled growth process, we have tuned the size (from <200 nm to >5 μm) as well as the morphology (from dumbbells-, to urchin- and needle-like) of this crystalline phase. Finally, we have performed the incorporation of Eu^{III} cations in the $LaPO_4$ *Rhabdophane* structure, where photophysical characterization demonstrates the formation of binary $LnPO_4$ solid solution phases.

2 Experimental

2.1 Chemicals

Lanthanum chloride heptahydrate ($LaCl_3{\cdot}7H_2O$), europium nitrate hexahydrate ($Eu(NO_3)_3{\cdot}6H_2O$), phosphoric acid (H_3PO_4), sodium chloride (NaCl), glycidol (Gly), and ethylene glycol (EG) were purchased from Sigma-Aldrich. Ethanol (EtOH) was purchased from Cicarelli. All chemicals were used as received. Milli-Q® water was employed in all cases.

2.2 Synthesis

Typically, precipitations were driven by aging at room temperature, from 2 to 24 h, aqueous solutions containing $LaCl_3$ and H_3PO_4 with the following concentrations: $[La^{III}] = [H_3PO_4] = 10$ mM; [HCl] = 250 mM, [NaCl] from 100 to 400 mM and [Gly] from 100 to 3400 mM. It is worth mentioning that the addition of hydrochloric acid ([HCl] = 250 mM) is used to guarantee the solubility of all chemical species at the beginning of the reaction. The tested solvents were water, EtOH, and EG. In the case of water:EtOH and water:EG mixtures, solutions were prepared with a determined volume of EtOH or EG so as to achieve concentrations of 25, 50 and 75% v/v; (% v/v defined as volume of non-aqueous solvents over total reaction volume).

The synthetic protocol is straightforward [35]: once the experimental conditions were defined (initial concentrations of each reagent), stock solutions were mixed either in glass or plastic vessels; Gly was added as the last reagent, since its addition triggers the start of the reaction. All the reactions were performed under continuous magnetic stirring. For all cases, the solids were collected by centrifugation (8000 RPM for 10 minutes), washed three times with a H_2O:EtOH solution of the same proportion (%v/v) as the precursor solution, and stored in absolute EtOH. Solids were dried at room temperature in a desiccator when necessary.

2.3 Precipitation pH profiles

Representative alkalinization (controls) and precipitation pH curves as a function of time were obtained by in situ potentiometric pH measurements. These were performed at room temperature under continuous magnetic stirring of aqueous media, exclusively.

2.4 Chemical and structural characterization of solids

The crystalline structure of the obtained solids was characterized by powder X-ray diffraction (PXRD), using a Panalytical Empyrean diffractometer with a graphite-filtered Cu Kα source (λ = 1.5406 Å). The morphology of the solids was determined by field emission scanning electron microscopy (FESEM) with a Carl Zeiss SUPRA 40 microscope; *ImageJ* software was employed to analyze the size distribution of obtained particles. FTIR spectra were collected in ATR mode, employing a Shimadzu Prestige 21 instrument. Thermogravimetric analysis (TGA) was performed in a TA Instruments SDT Q600 equipment, using alumina crucibles. The samples were heated, under inert atmosphere, from room temperature up to 800 °C (10 °C/min heating rate).

2.5 Photophysical characterization of solids

For the photophysical characterization, the powders obtained from the syntheses were air dried at room temperature. No further sample preparation was performed. Emission and excitation spectra of samples placed in quartz capillary holders were recorded using a PTI Inc. QuantaMaster QM4 spectrofluorimeter. Excitation spectra were measured by exciting the sample in the 220–500 nm interval while recording the emission at 590 nm. Emission spectra were measured in the 500–750 nm region, while exciting the sample at 295 or 394 nm. Schott filters WG345, OG570, and N4G were employed for all the measurements.

3 Results and discussion

As a first step to explore the synthesis of lanthanide phosphate samples, we carried out a detailed study of the precipitation process by following the pH profiles employing La^{III} as model lanthanide. Subsequently, the influence of the composition and viscosity of the solvent on

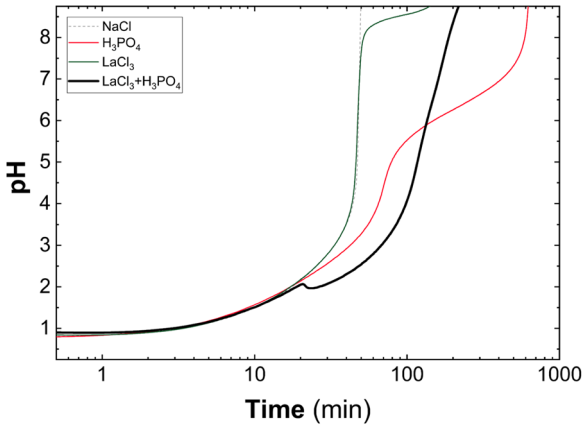

Fig. 1 pH evolution profiles recorded at room temperature employing [HCl] = 250 mM aqueous solutions containing: [Gly] = 1000 mM, [NaCl] = 250 mM (black dotted line), $[H_3PO_4]$ = 10 mM (red line) or $[La^{III}]$ = 10 mM (green line), and $[H_3PO_4]$ = 10 mM + $[La^{III}]$ = 10 mM (black line)

the morphology of the obtained phases was assessed (Scheme 1). Once the proper synthetic conditions to precipitate well-defined $LaPO_4$ particles were defined, we have explored the incorporation of Eu^{III} as a luminescent center and we characterized its effect on the photophysical properties.

Hence, firstly and with the objective of shedding light on the precipitation of lanthanum phosphate phases, in situ pH profiles were recorded at room temperature (Fig. 1). The dashed line in Fig. 1 depicts the pH profile for the control alkalinization experiment where Gly (the epoxide) was added to an aqueous solution containing HCl and NaCl, exclusively. As can be observed, after adding the epoxide, the pH increases reaching values higher than 9 in less than 60 minutes, even under this highly acidic initial condition ([HCl] = 250 mM). It is important to highlight that alkalinization and subsequent precipitation kinetics depend on the concentration of both Gly and chloride (the nucleophile), following: $v_{[OH-]} = k[\text{Gly}][Cl^-]$ [22, 29]. In the case of the second control experiment (red line), the initial mixture also contained phosphoric acid. After the addition of Gly, the reaction required tenfold additional time in comparison with the first control experiment (*ca.* 600 min), to reach pH values higher than 9. This difference is mainly due to the presence of an additional amount of a triprotic acid. As is observed in related systems [34], while in the first control experiment the pH profile resembles a strong acid (HCl) titration curve, the second example resembles the titration curve of a weak acid (H_3PO_4); furthermore the $[H_2PO_4^-]$:$[HPO_4^{2-}]$ buffer formation centered at around pH = 6.5 can be observed. In the last control experiment (green line) a solution containing H_3PO_4, HCl, and NaCl was tested. In this case, the addition of Gly results in a profile identical to the first control experiment up to *ca.* 50 min, where a slight change is observed. At that point, the pH curve splits from that of the HCl + NaCl control and a *plateau* centered around pH = 8.2 is noticeable. This event is followed by a white solid formation, attributed to lanthanum hydroxide precipitation in perfect agreement with its solubility product constant ($pK_{sp}^{La(OH)_3} = 18.7$) [36]. After these three control experiments, we have explored the precipitation kinetics of our target compound: $LaPO_4$ (black line). In this case, after adding Gly, the pH rises to an overshoot at pH = 2.06 followed by a *plateau* centered around pH = 1.96, while the formation of a white solid takes place. Interestingly, the precipitation occurs mainly in the presence of the triprotic and diprotic moieties from the phosphoric acid ($[H_3PO_4]$: $[H_2PO_4^-]$ = 1.23, see Fig. S1 in SI). After around 200 min, the pH sharply increases to pH > 9, indicating the absence of post precipitation events, recently observed for calcium phosphates [34]. In addition, the absence of a buffer zone around phosphoric acid's second acidic constant (pK_{a2}) indicates the quantitative precipitation of the phosphate moieties in the previous event. This characteristic pH profile is assigned to the $LaPO_4$ formation, in good agreement with its solubility product constant ($pK_{sp}^{LaPO_4} = 22.4$) [36]. Therefore, from these characteristic in situ pH profiles experiments, we can successfully confirm the formation of $LaPO_4$ at room temperature by employing the *Epoxide Route*. It is important to highlight that this feature arises as the most unique fingerprint of our synthetic method, allowing the "real-time" identification of the precipitation events [26, 30, 37].

To univocally identify the occurrence of the $LaPO_4$, the sample was characterized by PXRD, FTIR and TGA techniques. Figure 2A depicts the PXRD pattern of the sample, which is fully coincident with the *Rhabdophane* crystalline phase ($LaPO_4 \cdot \frac{2}{3}H_2O$). Moreover, ATR-FTIR analysis (Fig. 2B) supports this interpretation: the presence of water molecules is confirmed by the presence of a broad band at *ca.* 3500 cm^{-1} and a weak one at 1650 cm^{-1}, corresponding to the stretching and bending modes of OH moieties, respectively. Additionally, the bands centered at *ca.* 1000 cm^{-1} and 600 cm^{-1} are attributable to the stretching and bending modes of phosphate moieties, respectively [38]. Specifically, the triplet around 600 cm^{-1} can be ascribed to the antisymmetric stretching associated with the υ_4 vibration mode while the broad unresolved band corresponds to the υ_3 mode for a hydrated hexagonal *Rhabdophane* $LaPO_4$ [39]. Finally, TGA characterization confirms the presence of two kinds of water molecules in the solid material: the first one, physisorbed, which is released below 100 °C; and the second one, belonging to the *Rhabdophane* structure, that is lost at 200 °C [40]. Hence, the occurrence of *Rhabdophane* structure can be confirmed. In addition, PXRD and ATR-FTIR characterization of the calcined

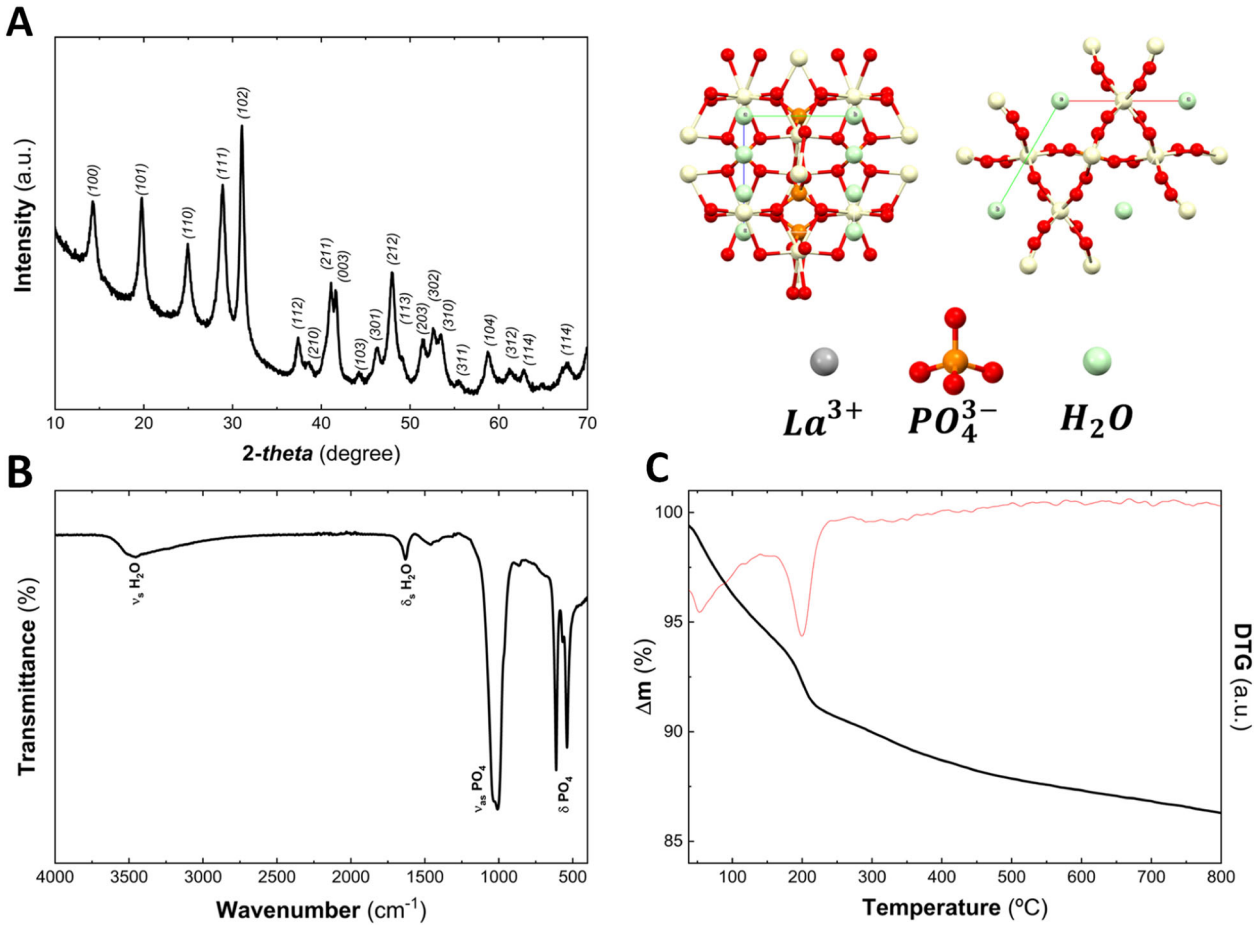

Fig. 2 PXRD patterns, without background subtraction, and crystallographic structure for *Rhabdophane* (**A**), ATR-FTIR spectrum (**B**), and TGA profile (**C**) for the $LaPO_4$ sample obtained at room temperature through the *Epoxide Route* from a solution containing: [HCl] = 250 mM, $[La^{III}]$ = $[H_3PO_4]$ = 10 mM, and [*Gly*] = 1000 mM

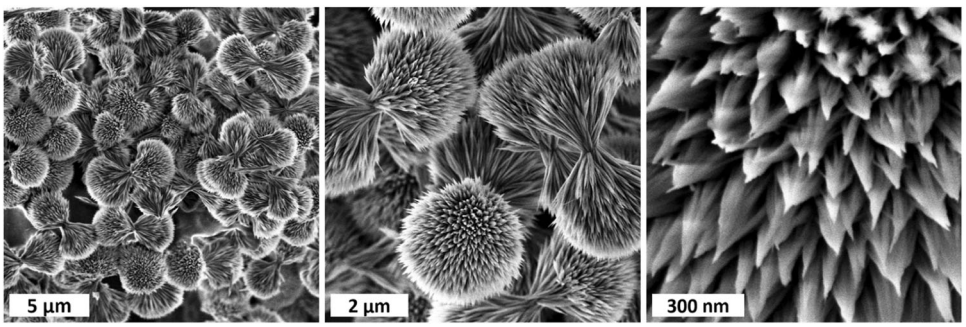

Fig. 3 FESEM images for the sample obtained by aging for 24 h at room temperature aqueous solutions containing: [HCl] = 250 mM, $[La^{III}]$ = $[H_3PO_4]$ = 10 mM, and [Gly] = 1000 mM

product confirms its transformation from the hexagonal *Rhabdophane* phase into the monoclinic *Monazite* phase, as expected (see Figs. S2 and S3, SI) [21].

Once the solid sample was chemically and structurally characterized, morphological aspects were assessed. Figure 3 depicts FESEM images of the obtained product, where the occurrence of the so-called dumbbell shaped particles approximately 5.6 µm long is observed. These polycrystalline systems consist of highly anisotropic needle/rod units about 2.7 µm long and about 90 nm wide, both exhibiting a narrow distribution. The occurrence of this peculiar morphology was already observed in numerous compounds and its origin is still a matter of debate [41]. Additionally, this remarkable length:thickness ratio is consistent with a highly anisotropic crystallographic growth, as was previously reported for layered hydroxides [35] and *Brushite* phase layered calcium phosphates [34] prepared by employing the *Epoxide Route*, positioning our synthetic method as a powerful approach for controlling anisotropic crystal growth.

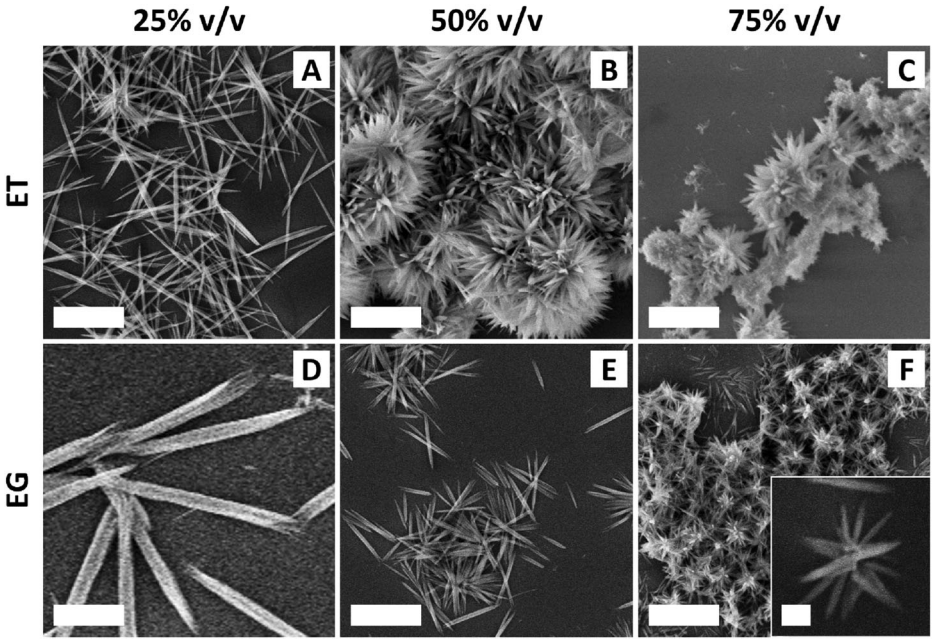

Fig. 4 FESEM images recorded for $LaPO_4$ samples synthesized at room temperature by employing [HCl] = 250 mM aqueous solutions containing: $[La^{III}] = [H_3PO_4] = 10$ mM, [Gly] = 1000 mM, and different proportions of cosolvents: EtOH (upper panel) and EG (lower panel). 25 (**A** and **D**), 50 (**B** and **E**) and 75% v/v (**C** and **F**) were used. Scale bar represents 500 nm in all cases, and 50 nm in the case of the inset in (**F**)

Recently we have observed that for the synthesis of amorphous calcium phosphate nanospheres, the use of green viscous solvents such as EG and glycerol could be employed as a new tool to control the size of the particles, as well as their internal structure [34]. Hence, keeping this in mind, we decided to extend the use of organic co-solvents as a tool for controlling size and shape in the synthesis of $LaPO_4$ particles. For that, we opted for the employment of EtOH and EG as cosolvents of water in the initial synthetic mixture, as two representative members of the "non-viscous" and "viscous" family of solvents, respectively. Figure 4 depicts the FESEM images recorded for the set of experiments carried out by employing 25, 50, and 75% (v/v) of EtOH (upper panel) or EG (lower panel). Interestingly, in both cases the increment in the organic co-solvent proportion triggers the transition from isolated needle-like/rod particles (Fig. 4A, D) to urchin-like ones (Fig. 4B, C, E, F). These results could be related to a reduction in the dielectric constant of the solvent mixture (as the proportion of organic co-solvent increases) affecting the colloidal stability of the growing seeds. This effect would proceed via agglomeration of the primary units and subsequent growth, resulting in the final formation of polycrystalline particles. Moreover, the viscosity also affects these two morphologies. For instance, in the case of experiments performed with 25% of organic co-solvent (needle-like morphology), a size reduction of around five-fold to tenfold is observed in comparison with experiments carried out in aqueous solution. Moreover, experiments recorded with 75% of organic co-solvent (urchin-like morphology) exhibit a marked downsizing around 50-fold by solvent replacement. It is worth mentioning that these experiments provide the first evidence that the viscous solvent-controlled growth process that we have recently reported for amorphous calcium phosphate spherical nanoparticles [34] can also take place in the case of highly anisotropic particles, where the solvent mixture induces significant morphology changes, apart from those related to the size.

Taking into account the possibility of synthesizing pure $LaPO_4$ with controlled size and morphology, we proceeded to explore the incorporation of Eu^{III} cations as luminescent ion guests into this inorganic host matrix, with the goal of obtaining a representative family of $La_{1-x}Eu_xPO_4$ solid solutions. Figure 5 depicts the FESEM images of the samples obtained, where it can be observed that, in all the cases, the size and morphology observed for La^{III} based particles are preserved. Additionally, while PXRD characterization confirms the occurrence of *Rhabdophane*-like structures, EDS analysis confirms the quantitative incorporation of Eu in all cases (Fig. S4, SI).

Finally, to further confirm the incorporation of Eu^{III} in the *Rhabdophane*-like structure, we have characterized the $La_{1-x}Eu_xPO_4$ ($x = 0.1$) samples in terms of their luminescent (excitation/emission) properties. The recorded emission spectra (Fig. 6) of Eu^{III} cations is in excellent agreement with the relative intensities recorded for hydrothermally aged Eu@$LaPO_4$ phases [19]. The emission spectrum features the $^5D_0 \rightarrow {}^5F_J$ ($J = 1, 2, 3, 4$) transition of Eu^{III} evidenced by the corresponding peaks located at 585, 591 ($^5D_0 \rightarrow {}^7F_1$), 612, 619 ($^5D_0 \rightarrow {}^7F_2$), 650 ($^5D_0 \rightarrow {}^7F_3$), 683, and 694 ($^5D_0 \rightarrow {}^7F_4$) nm. Among these emission lines, the magnetic-dipole transition $^5D_0 \rightarrow {}^7F_1$ (591 nm) is the most intense set, characterized by orange-red emission.

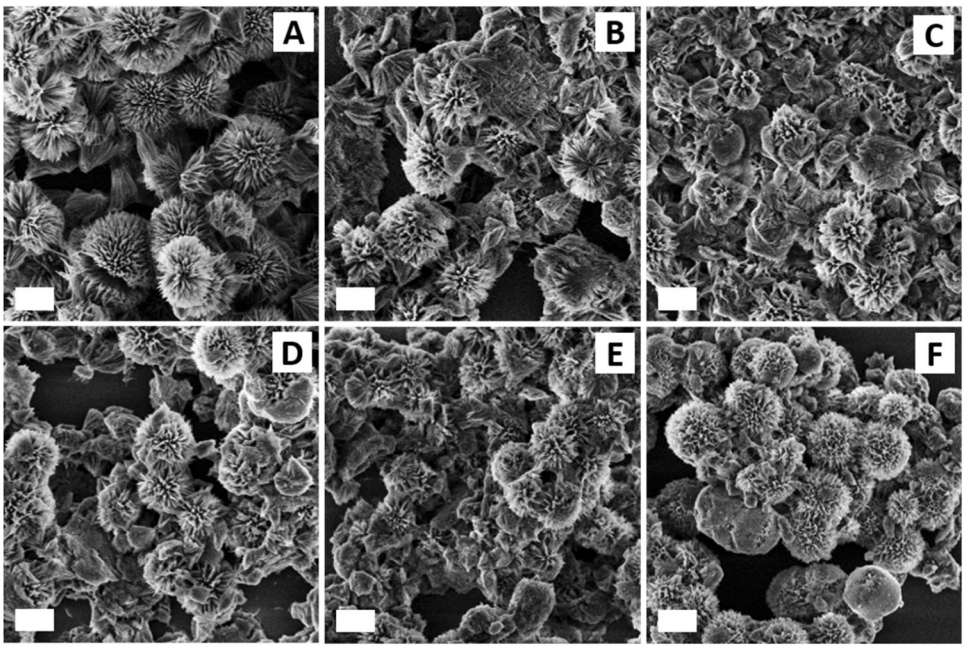

Fig. 5 FESEM images recorded for $La_{1-x}Eu_xPO_4$ samples obtained through the *Epoxide Route* by employing [HCl] = 250 mM aqueous solutions containing $[La^{III} + Eu^{III}]$ = 10 mM, $[H_3PO_4]$ = 10 mM, [NaCl] = 400 mM, [Gly] = 1300 mM, and *x*: 0 (**A**), 0.05 (**B**), 0.10 (**C**), 0.15 (**D**), 0.20 (**E**) and 1 (**F**). Scale bar represents 1 µm in all cases

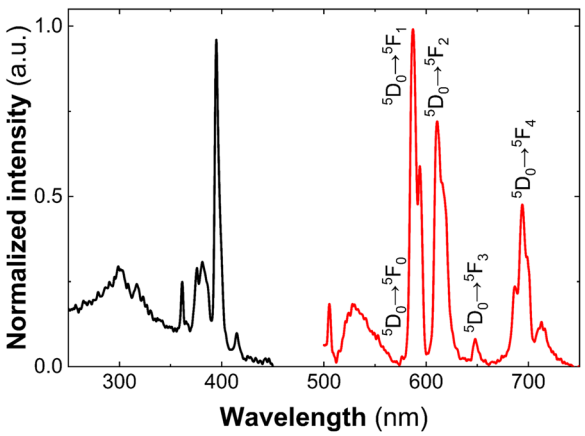

Fig. 6 Excitation (black line) and emission spectra (red line) for $La_{1-x}Eu_xPO_4$ with x = 0.1 obtained through the *Epoxide Route* at room temperature

Furthermore, the intensity of the transitions between different *J*-number levels depends on the symmetry of the local environments of Eu^{III} centers, typically described in terms of the Judd-Ofelt theory. This behavior was also observed for other Eu^{III} contents in the solid, demonstrating that this emissive ion isomorphically substitutes La^{III} positions within the lattice, in the form of a solid solution. These results establish the Epoxide Route as an alternative one-pot room temperature approach for obtaining luminescent materials based on Eu^{III} with physicochemical properties comparable to their hydrothermally synthesized analogs.

Additionally, having demonstrated the efficiency of the *Epoxide Route* for obtaining multi-lanthanide phosphate samples, we have characterized the luminescent properties of calcined samples, i.e.: *Monazite* structure obtained after calcining the *Rhabdophane* materials up to 900 °C (see Fig. S5, SI). The spectrum for the Monazite-like sample exhibits an enhancement of the intensity of the bands associated with the magnetic ($^5D_0 \rightarrow {}^7F_1$) transitions in comparison with the *Rhabdophane*-like sample. Specifically, this result suggests a more intense magnetic-dipole transition ($^5D_0 \rightarrow {}^7F_1$) associated with Eu^{III} ions located at sites with inversion symmetry, as expected (see SI for more details) [19, 21, 35].

4 Conclusions

In this work, we have demonstrated that the *Epoxide Route* constitutes an excellent alternative for synthesizing lanthanide phosphates with different morphologies and compositions. In particular, we showed that *Rhabdophane* phase of $LaPO_4$ can be synthesized at room temperature using this simple experimental procedure. In addition, thanks to the versatility of the *Epoxide Route*, we were able to identify the events that lead to the formation of this phase by simple in situ experiments, such as following the reaction progress using a pH-meter. Furthermore, we have demonstrated that the previously reported solvent-controlled growth approach has a distinct effect over the final material morphology, allowing crystalline particles with dumbbell, urchin and needle shapes to be obtained, with sizes that ranged from less than 200 nm to more than 5 µm. Finally, the synthetic method was adapted to incorporate Eu^{III} cations within the $LaPO_4$ structure, allowing monophasic luminescent materials obtaintion.

In summary, the results presented in this work demonstrate that the *Epoxide Route* offers a straightforward preparative path for obtaining pure and well-crystallized lanthanum phosphates and their Eu(III) substituted solid solutions, paving the way to the simple production of luminescent materials for which a wide variety of applications can be envisioned.

Data availability

Data are available from the authors.

Acknowledgements This work was supported by University of Buenos Aires (UBACyT 20020130100610BA for MJ & 2002017010755BA for BCB), Agencia Nacional de Promoción Científica y Tecnológica (ANPCyT PICT 2012-1167 for MJ), Fundación Argentina de Nanotecnología (Proyecto Presemillas for BCB) and National Research Council of Argentina (CONICET PIP 11220170100991CO for MJ). Authors thanks Dr. Claudia Marchi for her remarkable help in the FESEM images. VO is a member of ALN.

Funding University of Buenos Aires (UBACyT 20020130100610BA for MJ, UBACyT 2002017010755BA for BCB). Fundación argentina de Nanotecnología, FAN- Proyecto Presemillas (for BCB). Agencia Nacional de Promoción Científica y Tecnológica (ANPCyT PICT 2012-1167 for MJ). National Research Council of Argentina (CONICET PIP 11220170100991CO for MJ). Open Access funding provided thanks to the CRUE-CSIC agreement with Springer Nature.

Compliance with ethical standards

Conflict of interest The authors declare no competing interests.

Publisher's note Springer Nature remains neutral with regard to jurisdictional claims in published maps and institutional affiliations.

References

1. Moine B, Bizarri G (2006) Why the quest of new rare earth doped phosphors deserves to go on. Opt Mater 28(1):58–63
2. Escudero A, Becerro AI, Carrillo-Carrión C, Núñez NO, Zyuzin MV, Laguna M et al. (2017) Rare earth based nanostructured materials: synthesis, functionalization, properties and bioimaging and biosensing applications. Nanophotonics 6(5):881–921
3. Eliseeva SV, Bünzli J-CG (2009) Lanthanide luminescence for functional materials and bio-sciences. Chem Soc Rev 39(1):189–227
4. Baranovskaya VB, Karpov YUA, Petrova KV, Korotkova NA (2021) Actual trends in the application of rare-earth metals and their compounds in the production of magnetic and luminescent materials: a review. Russ J Non-Ferr Met 62(1):10–31
5. Lucas J, Lucas P, Le Mercier T, Rollat A, Davenport W. Chapter 16 - applications of rare earth luminescent materials. In: Lucas J, Lucas P, Le Mercier T, Rollat A, Davenport W, editors. Rare earths. Amsterdam: Elsevier; 2015. p. 281–318. https://www.sciencedirect.com/science/article/pii/B9780444627353000152
6. Sorbello C, Barja BC, Jobbágy M (2014) Monodispersed Ce (IV)–Gd(III)–Eu(III) oxide phosphors for enhanced red emission under visible excitation. J Mater Chem C 2(6):1010–1017
7. Achary SN, Bevara S, Tyagi AK (2017) Recent progress on synthesis and structural aspects of rare-earth phosphates. Coord Chem Rev 340:266–297
8. Chen GH, Kang XL, Yang Y (2014) Luminescence properties of rare-earth co-doped phosphate glasses for white light emitting diodes. Adv Mater Res 989–994:369–372
9. Hachani S, Guerbous L (2019) Synthesis, luminescence, and energy transfer properties of YPO4:Gd3+, Eu3+ and YP3O9:Sm3+, Eu3+ phosphors. J Fluoresc 29(3):665–672
10. Tamboli S, Nair GB, Dhoble SJ, Swart HC. Versatile applications of rare-earth activated phosphate phosphors: a review. In: Luminescent materials in display and biomedical applications. CRC Press; 2020. https://doi.org/10.1201/9780429025334-2
11. Weber MJ. Chapter 35 Rare earth lasers. In: Handbook on the physics and chemistry of rare earths. Elsevier; 1979. p. 275–315. https://www.sciencedirect.com/science/article/pii/S0168127379040083
12. Runowski M, Shyichuk A, Tymiński A, Grzyb T, Lavín V, Lis S (2018) Multifunctional optical sensors for nanomanometry and nanothermometry: high-pressure and high-temperature upconversion luminescence of lanthanide-doped phosphates—LaPO4/YPO4:Yb3+–Tm3+. ACS Appl Mater Interfaces 10 (20):17269–17279. May 23
13. Rao RP, Devine DJ (2000) RE-activated lanthanide phosphate phosphors for PDP applications. J Lumin 87–89:1260–1263
14. Komban R, Beckmann R, Rode S, Ichilmann S, Kühnle A, Beginn U et al. (2011) Surface modification of luminescent lanthanide phosphate nanorods with cationic "Quat-primer" polymers. Langmuir. 27(16):10174–10183
15. Schuetz P, Caruso F (2002) Electrostatically assembled fluorescent thin films of rare-earth-doped lanthanum phosphate nanoparticles. Chem Mater 14(11):4509–4516
16. Hutchison AJ (1999) Calcitriol, lanthanum carbonate, and other new phosphate binders in the management of renal osteodystrophy. Perit Dial Int 19(Suppl 2):S408–412
17. Binnemans K (2015) Interpretation of europium(III) spectra. Coord Chem Rev 295:1–45
18. Reisfeld R, Zigansky E, Gaft M (2004) Europium probe for estimation of site symmetry in glass films, glasses and crystals. Mol Phys 102(11–12):1319–1330
19. Yang M, You H, Jia G, Huang Y, Song Y, Zheng Y et al. (2009) Selective synthesis of hexagonal and monoclinic LaPO4:Eu3+ nanorods by a hydrothermal method. J Cryst Growth 311 (23):4753–4758
20. Kang YC, Kim EJ, Lee DY, Park HD (2002) High brightness LaPO4:Ce,Tb phosphor particles with spherical shape. J Alloy Compd 347(1):266–270
21. Chaudan E, Kim J, Tusseau-Nenez S, Goldner P, Malta OL, Peretti J et al. (2018) Polarized luminescence of anisotropic LaPO4:Eu nanocrystal polymorphs. J Am Chem Soc 140 (30):9512–9517
22. Oestreicher V, Jobbágy M (2013) One pot synthesis of Mg2Al (OH)6Cl·1.5H2O layered double hydroxides: the Epoxide Route. Langmuir 29(39):12104–12109

23. Tokudome Y (2017) Aqueous synthesis of metal hydroxides with controllable nano/macro architectures. J Ceram Soc Jpn 125 (8):597–602
24. Tokudome Y, Nakanishi K, Kanamori K, Fujita K, Akamatsu H, Hanada T (2009) Structural characterization of hierarchically porous alumina aerogel and xerogel monoliths. J Colloid Interface Sci 338(2):506–513
25. Arencibia N, Oestreicher V, A Viva F, Jobbágy M (2017) Nanotextured alpha Ni(ii)–Co(ii) hydroxides as supercapacitive active phases. RSC Adv 7(10):5595–5600
26. Oestreicher V, Hunt D, Torres-Cavanillas R, Abellán G, Scherlis DA, Jobbágy M (2019) Halide-mediated modification of magnetism and electronic structure of α-Co(II) hydroxides: synthesis, characterization, and DFT+U simulations. Inorg Chem 58 (14):9414–9424
27. Oestreicher V, Hunt D, Dolle C, Borovik P, Jobbágy M, Abellán G et al. (2021) The missing link in the magnetism of hybrid cobalt layered hydroxides: the odd–even effect of the organic spacer. Chem Eur J 27(3):921–927
28. Tokudome Y, Morimoto T, Tarutani N, Vaz PD, Nunes CD, Prevot V et al. (2016) Layered double hydroxide nanoclusters: aqueous, concentrated, stable, and catalytically active colloids toward green chemistry. ACS Nano 10(5):5550–5559
29. Oestreicher V, Fábregas I, Jobbágy M (2014) One-pot epoxide-driven synthesis of M2Al(OH)6Cl·1.5H2O layered double hydroxides: precipitation mechanism and relative stabilities. J Phys Chem C 118(51):30274–30281
30. Oestreicher V, Jobbágy M (2019) On demand one-pot mild preparation of layered double hydroxides and their hybrid forms: advances through the Epoxide Route. Chem Eu J 25 (54):12611–12619
31. Oestreicher V, Perullini M, Jobbágy M (2016) Physicochemical aspects of epoxide driven nano-ZrO2 hydrogel formation: milder kinetics for better properties. Dalton Trans 45(24):9920–9924
32. Oestreicher V, Jobbágy M (2017) Extremely efficient crystallization of HKUST-1 and Keggin-loaded related phases through the epoxide route. Chem Commun 53(24):3466–3468
33. Oestreicher V, Huck-Iriart C, Soler-Illia G, Angelomé PC, Jobbágy M (2020) Mild homogeneous synthesis of gold nanoparticles through the epoxide route: kinetics, mechanisms, and related one-pot composites. Chem Eur J 26(14):3157–3165
34. Borovik P, Oestreicher V, Huck-Iriart C, Jobbágy M (2021) Chem Eur J 27:10077. https://doi.org/10.1002/chem.202005483
35. Gupta SK, Ghosh PS, Sahu M, Bhattacharyya K, Tewari R, Natarajan V (2015) Intense red emitting monoclinic LaPO4:Eu3+ nanoparticles: host–dopant energy transfer dynamics and photoluminescence properties. RSC Adv 5(72):58832–58842
36. Dean JA, Lange NA. Lange's handbook of chemistry. McGraw-Hill; 1999. p 1538
37. Tarutani N, Tokudome Y, Jobbágy M, Soler-Illia GJAA, Takahashi M (2019) Mesoporous microspheres of nickel-based layered hydroxides by aerosol-assisted self-assembly using crystalline nano-building blocks. J Sol-Gel Sci Technol 89(1):216–224
38. Clavier N, Mesbah A, Szenknect S, Dacheux N (2018) Monazite, rhabdophane, xenotime & churchite: vibrational spectroscopy of gadolinium phosphate polymorphs. Spectrochim Acta Part A: Mol Biomolecular Spectrosc 205:85–94
39. Kijkowska R, Cholewka E, Duszak B (2003) X-ray diffraction and Ir-absorption characteristics of lanthanide orthophosphates obtained by crystallisation from phosphoric acid solution. J Mater Sci 38(2):223–228
40. Oestreicher V, Abellán G, Coronado E (2020) The role of covalent functionalization in the thermal stability and decomposition of hybrid layered hydroxides. Phys Status Solidi (RRL) – Rapid Res Lett 14(12):2000380
41. Prymak O, Sokolova V, Peitsch T, Epple M (2006) The crystallization of fluoroapatite dumbbells from supersaturated aqueous solution. Cryst Growth Des 6(2):498–506